Glacial to interglacial changes in the settling depth of the Mediterranean Outflow plume

M. Rogerson,[1] E. J. Rohling, P. P. E. Weaver, and J. W. Murray
Southampton Oceanography Centre, Southampton, UK

Received 28 October 2004; revised 12 April 2005; accepted 21 April 2005; published 19 August 2005.

[1] We present micropalaeontological and grain-size records for a set of sediment cores from the Gulf of Cadiz (southwest Spain) that reflect changes in the position and strength of the Mediterranean Outflow (MO) current. The cores sample a sediment drift (the Gil Eanes Drift) that is positioned lower on the slope in the Gulf of Cadiz than the position of the main current today. The data indicate that the drift is of glacial age and that the glacial MO current was positioned lower on the slope than today but also that it was active over a considerably reduced area of the slope. We argue that this observation is consistent with physical constraints on the Gibraltar Exchange and on the likely settling and spreading behavior of the MO plume along the Iberian Margin under glacial environmental and sea level conditions. The deeper settling of the MO is likely to have influenced the formation of glacial North Atlantic Intermediate Water and also may have exerted indirect influence on the formation of glacial North Atlantic Deep Water.

Citation: Rogerson, M., E. J. Rohling, P. P. E. Weaver, and J. W. Murray (2005), Glacial to interglacial changes in the settling depth of the Mediterranean Outflow plume, *Paleoceanography*, *20*, PA3007, doi:10.1029/2004PA001106.

1. Introduction

[2] The Gulf of Cadiz (GoC) lies to the southwest of the Iberian Peninsula, at the western end of the Strait of Gibraltar, where density driven exchange occurs between the Mediterranean Sea and the Atlantic Ocean. Here dense Mediterranean waters flow westward at depth to form the Mediterranean Outflow current (MO) and relatively fresh Atlantic water flows eastward at the surface to form the Atlantic Inflow current (AI). This exchange is part of the antiestuarine circulation in the Mediterranean basin that is driven primarily by high net evaporation in the eastern Mediterranean [*Bryden and Stommel*, 1984]. Having passed through the strait, the MO flows down the slope of the GoC and into the North Atlantic. Within the GoC the MO branches, forming two separate flow cores at 500–800 m and 1000–1500 m [*Iorga and Lozier*, 1999; *Borenas et al.*, 2002; *Johnson et al.*, 2002]. As the flow passes over the slope of the GoC, it causes deposition of a large contourite drift [*Kenyon and Belderson*, 1973].

[3] The deeper branch of the current (MO2) forms a large plume of warm, saline water that reaches as far west as the Azores [*Alves et al.*, 2002], and elevated salinities that may be attributed to it can be found at the Bahama Bank [*Armi and Bray*, 1982]. Another part of this deeper water (MO2) follows the same course as the shallower flow core (MO1) into the northern North Atlantic [*Iorga and Lozier*, 1999] (see Figure 1). The shallower, more onshore flow core (MO1) passes along the Portuguese margin [*Iorga and Lozier*, 1999] and eventually penetrates at least as far north as the Rockall Trough [*Hill and Mitchelson-Jacob*, 1993]. Figure 1 shows both the main flow paths and the resultant salinity field of the Mediterranean plume in the North Atlantic. Though it has been postulated that MO1 shoals sufficiently to pass into the Greenland-Iceland-Norwegian (GIN) seas [*Reid*, 1979], it is now believed that the sill of the Wyville-Thomson Ridge is too shallow (500 m) for the MO to cross and that it is recirculated into the northern North Atlantic [*Hill and Mitchelson-Jacob*, 1993]. Salt supplied to the northern North Atlantic surface waters by the MO may promote the development of negative buoyancy in the nascent North Atlantic Intermediate Water, which forms south of Iceland [*Pickard and Emery*, 1990], and may indirectly impact on the salinity of the nascent North Atlantic Deep Water by mixing with overlying water masses in the Rockall Trough. Indeed, altered salinity in the MO has been shown to strongly impact on the North Atlantic meridional overturning in a manner analogous to that suggested by Reid in a general circulation model [*Rahmstorf*, 1998].

[4] Seismic sections from the GoC contourite drift show an alternating series of highly reflective and acoustically transparent layers, and sediment core studies have shown that these represent paired layers of sand and mud [*Nelson et al.*, 1993; *Rodero et al.*, 1999]. Radiocarbon dating of the most recent pair indicates that the sand deposition started at the onset of the Younger Dryas, so that the underlying mud layer represents a glacial facies [*Nelson et al.*, 1993]. The oldest ages obtained for the onset of sand deposition in other cores were representative of the last deglaciation (~16 kyr B.P. [*Stow et al.*, 1986]). Each sand-mud pair was found to represent a glacial cycle [*Stow et al.*, 1986; *Nelson et al.*, 1993; *Nelson et al.*, 1999], suggesting that during interglacials the MO plume is in a similar position to that

[1] Now at Faculty of Geoscience, University of Utrecht, Utrecht, Netherlands.

0883-8305/05/2004PA001106$12.00

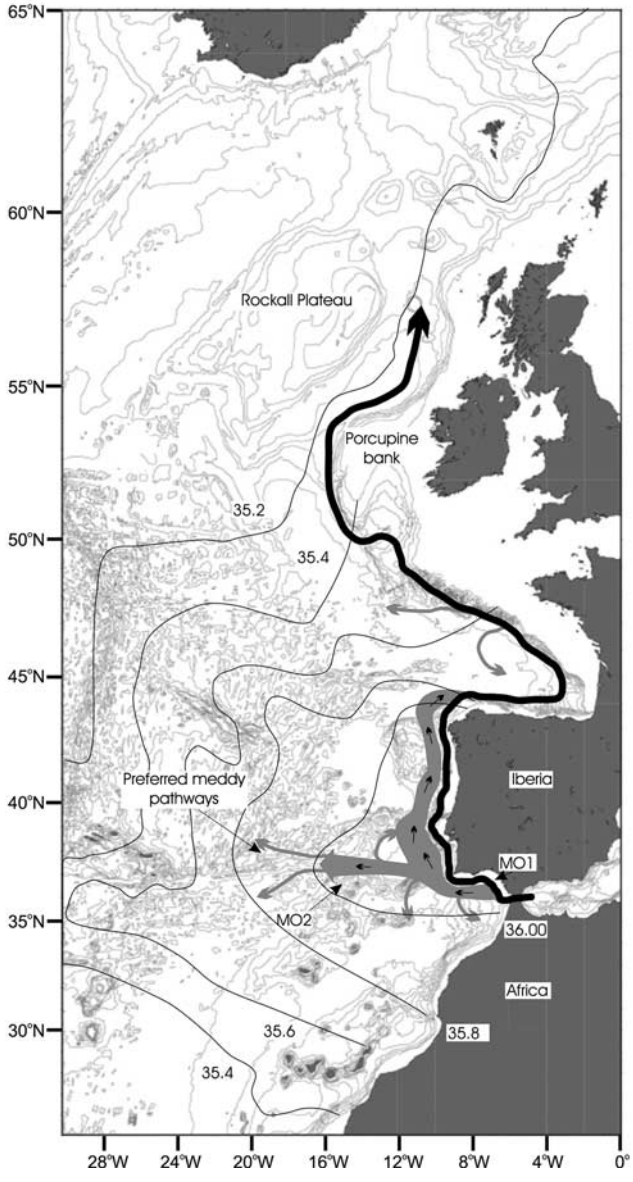

Figure 1. Summary of the Mediterranean Outflow (MO) in the eastern North Atlantic. The main flow paths of MO1 and MO2 are taken from *Iorga and Lozier* [1999]. Contours show salinity of Mediterranean Outflow as defined by *Reid* [1979] (in parts per million).

observed today, whereas it is absent from the slope when sea level falls more than 50 m below the present level [*Nelson et al.*, 1993, 1999]. It has been postulated that this indicates an absence of water mass exchange through the Strait of Gibraltar at glacial times [*Nelson et al.*, 1993]. Conversely, continuing albeit reduced MO flow during the last glacial period has been inferred from sedimentological and chemical proxy data for the Portuguese margin [*Hall and McCave*, 2000; *Schönfeld and Zahn*, 2000; *Moreno et al.*, 2002]. It has also been suggested that the flow deeper than 2000 m may have been enhanced at glacial times, because of an intensified lower flow core (MO2) [*Thomson et al.*, 1999; *Schönfeld and Zahn*, 2000]. In addition, some evidence for current activity has been reported on the GoC slope from a small number of narrow and discrete channels [*Mulder et al.*, 2002].

[5] Modeling studies [*Bigg*, 1995; *Myers et al.*, 1998; *Rohling*, 1999; *Myers*, 2002] and reconstructions based on paleoceanographic proxy data [*Thunell and Williams*, 1989; *Rohling*, 1994; *Rohling and Bryden*, 1994; *Rohling and De Rijk*, 1999; *Schönfeld and Zahn*, 2000] indicate that the Mediterranean has experienced antiestuarine circulation similar (in sign) to that of today throughout the last 30,000 years, with the only possible (debated) exception being the period of deposition of early Holocene sapropel S1 in the eastern Mediterranean (9–6 kyr B.P.). This argues against on/off switching of the MO flow on glacial/interglacial timescales as proposed by *Nelson et al.* [1993]. The causes for absence of the MO flow from its present course in the GoC during sea level lowstands should therefore be sought in shifts of the flow's position on the continental slope. The present study uses the sedimentary characteristics, microfossil abundance data and stable isotope records from sediment cores recovered from the Gulf of Cadiz to reconstruct the position, flux and influence of the MO during the Last Glacial Maximum (LGM).

2. Background

2.1. Physical Constraints on the MO Plume

2.1.1. Volume Flux and Salinity of Outflow

[6] To understand the history of the MO plume, we first examine the physical constraints on its behavior. The shallow (284 m) and narrow (~14 km) Strait of Gibraltar limits the amount of water mass exchange between the Mediterranean and the Atlantic. The two-layer flow in the Strait has been shown to reach supercritical values (i.e., the two-layer Froude number equals/exceeds 1) during almost every tidal cycle, and approximately half of the MO flux is achieved under critical flow during the falling tide [*Bryden et al.*, 1988]. The Gibraltar Exchange may thus practically be assumed to be maximal or very near maximal [*Bryden et al.*, 1988; *Bryden and Kinder*, 1991]. Under lower sea level conditions, as have existed in the past, the exchange is likely to have been maximal throughout the tidal cycle [*Rohling and Bryden*, 1994; *Matthiesen and Haines*, 2003].

[7] Under maximal exchange conditions, assuming the Camarinal sill (see Figure 2) is triangular in cross section, the fluxes of the MO and AI can be considered [*Bryden and Kinder*, 1991] according to

$$Q_{AI} - Q_{MO} = C(D_s\ b_s/2)\sqrt{(g'\ D_s)}. \qquad (1)$$

Here Q_{AI} is the flux of AI, Q_{MO} is the flux of MO, b_s is sill width, D_s is water depth at the sill, g' is reduced gravity. The reduced gravity is determined as $g' = g\beta(S_{MO} - S_{AI})$ where S_{MO} and S_{AI} are the salinities of MO and AI waters respectively, β is the coefficient of saline contraction determined from the equation of state for seawater, and C is a constant that depends on the physical configuration of the strait (~0.28 in this case) [*Bryden*, 1993]. Combining equation (1) with statements of salt and mass conservation, it is possible to show that the salinity contrast between the

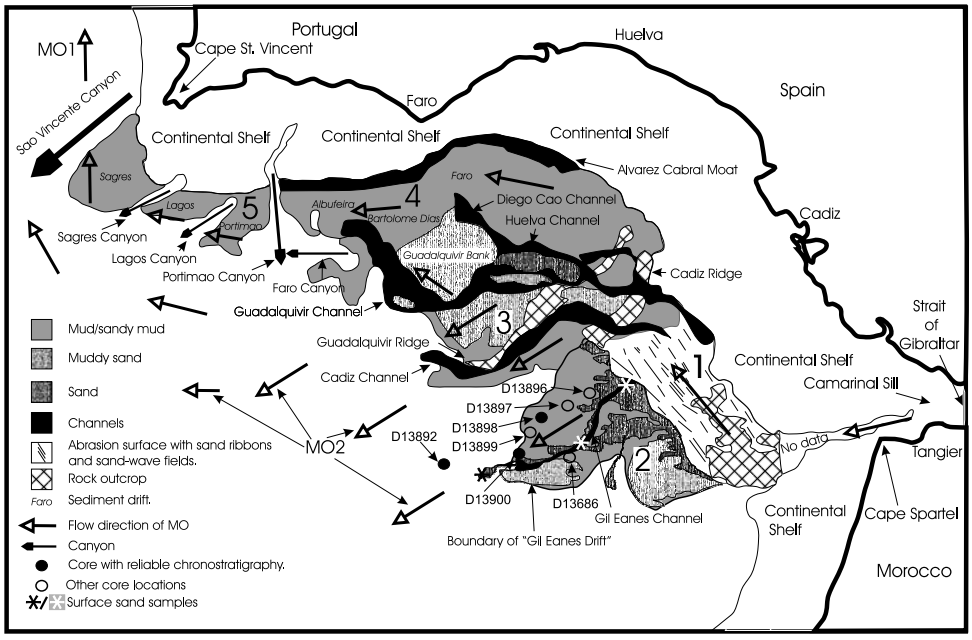

Figure 2. Sediment facies of the Gulf of Cadiz contourite drift as revealed by side-scan sonar data. Core locations are indicated. After *Hernandez-Molina et al.* [2003].

Mediterranean and Atlantic at Gibraltar is determined by net evaporation in the Mediterranean and the depth and width of the sill [*Bryden*, 1993]:

$$(S_{AI} - S_{MO})^{3/2} = C\ E/((b_s\ Ds)\sqrt{D_s}). \qquad (2)$$

Here E is net evaporation over the Mediterranean basin. Lowering sea level will therefore decrease the exchange through the Strait of Gibraltar by decreasing both D_s and b_s, thereby reducing the flux and increasing the salinity of the MO.

[8] The maximum flux of Mediterranean water through the Strait of Gibraltar during the Last Glacial Maximum (LGM) has been calculated at ~0.3 Sv [*Rohling and Bryden*, 1994; *Matthiesen and Haines*, 2003], less than half that measured today (0.79 Sv [*Bryden and Kinder*, 1991]), assuming no change in net evaporation from the Mediterranean (E). Basin average E is expected to be roughly similar to today, though its spatial distribution may have been altered [*Bigg*, 1994, 1995; *Myers et al.*, 1998], and so the actual LGM flux will have been close to this estimate. Proportional changes in flux to those shown by *Rohling and Bryden* [1994] are found in a numerical model of the internal circulation of the Mediterranean during the LGM [*Myers et al.*, 1998]. A transport of 0.32 Sv would be associated with more than a doubling in the salinity contrast across the Strait of Gibraltar ($S_1 - S_2$), which is 1.9 psu today [*Bryden et al.*, 1988], to an estimated 4.1 psu during the LGM [*Rohling and Bryden*, 1994]. The inference of increased Mediterranean salinity is supported by the observation of enriched $\delta^{18}O$ in the tests of planktonic foraminifera during the LGM, particularly in the Levantine basin [*Rohling*, 1999; *Rohling and De Rijk*, 1999].

[9] As the MO leaves the Strait of Gibraltar, it rapidly descends the slope as a result of its high negative buoyancy and its downslope velocity is controlled by the reduced gravity (g'). An increased glacial Mediterranean-Atlantic salinity contrast would have enhanced g', which would in turn have caused the MO plume to settle to greater depths in the GoC and wider Atlantic, relative to the present. It is relevant therefore to briefly consider the processes that govern the characteristics of the MO plume.

2.1.2. Settling, Entrainment, and Dimensions of the MO Plume

[10] The MO entrains Atlantic water as it passes into the GoC, increasing in volume by a factor of 3 to 4 within the first 100 km of leaving the Strait of Gibraltar [*O'Neill-Baringer and Price*, 1999]. This reduces its negative buoyancy and erodes the velocity of the plume. The final depth of settling of the MO plume is controlled by the final density of the MO product water (equal to $a\rho_{MO} + b\rho_{atl}$ where ρ_{MO} and ρ_{atl} are the densities of the initial MO and the ambient Atlantic waters respectively, and a and b are the fractions of Mediterranean and Atlantic water in the final plume ($a + b = 1$)). Today, the plume is characterized by b/a values in the order of 2 to 3 [*O'Neill-Baringer and Price*, 1999].

[11] In essence, Mediterranean water is evaporated Atlantic water. Therefore ρ_{MO} is determined by ρ_{atl} and E, so that the effects of variations in ρ_{atl} will be reflected in ρ_{MO} and will not materially influence g'. However, there is an up to 2°C temperature range between the waters mixed into the upper and lower parts of the MO plume during the crucial period of high entrainment within 100 km of its exit from the Strait of Gibraltar, and the final density of the top of the plume is therefore lower than that of the bottom [*O'Neill-Baringer and Price*, 1999]. This results in g' being variable vertically within the MO plume, with the lowermost parts of

the MO water displaying slightly stronger negative buoyancy than the uppermost part. The vertical range of Atlantic water densities incorporated into the MO plume can be termed $\Delta\rho_{atl}$, and causes some minor lateral spreading within the plume which is exaggerated by topography on the GoC slope [*Borenas et al.*, 2002].

[12] Entrainment of Atlantic water into the MO plume is gradual, and mixing occurs in the outermost (uppermost) part of the plume before it penetrates the flow core. A layer of almost pure Mediterranean water can thus be found at the base of the MO on the GoC slope beyond the immediate vicinity of the Strait of Gibraltar. On average, the height of the unmixed layer is less than half of that of the height of frictional influence (Ekman layer) from the bottom [*Johnson et al.*, 1994]. In areas with a high ratio of height (H) over the thickness of the Ekman layer ($D = \pi(2A/f)^{1/2}$ where A is the eddy viscosity coefficient and f is the Coriolis parameter), the bottom layer will be laterally sheared to move at an angle relative to the rest of the plume (up to 45° if $H/D = {}^1/_2$ [*Gammelsrod*, 1975]), which causes lateral spreading. As the plume thins into the GoC, H/D decreases and the angle of veering also decreases, reducing the tendency of the plume to spread as it passes into the North Atlantic. In addition to the direct influence of this shearing, which is termed Ekman veering, friction acts on the plume as a whole, generally causing the flow to spread laterally and descend the slope [*O'Neill-Baringer and Price*, 1999]. The magnitude of the frictional force is largely dependent on bottom drag and plume height [*Price and O'Neill-Baringer*, 1994].

[13] The height of the MO plume (H) will be related to the flux. The thickness of the Ekman layer (D) will not vary significantly through time, so that the effect of reducing H will be to decrease the angle of veering, thus reducing the amount of spreading. Reduced H will also decrease $\Delta\rho_{atl}$, thus further reducing the tendency of the plume to spread laterally. Stream tube models suggest that the splitting of the flow into MO1 and MO2 is probably caused by the high topography of the GoC slope acting on the MO current as it spreads laterally [*Borenas et al.*, 2002], and it therefore can be expected that reduced spreading would diminish the capability of topography to split the flow. Consequently, we expect the MO to form a narrower, more coherent (single?) plume of water during the LGM, compared to the present.

[14] The above schematic representation will be complicated by temporal variability in the proportion of mixing in the first 100 km from the Strait of Gibraltar (b/a). A smaller MO flux may mix more vigorously with ambient Atlantic water and lose its negative buoyancy faster, as it would have a greater surface area relative to its volume. It is therefore likely that past b/a will be altered from that of today. If b/a is not constant, the final settling depth of the plume does not vary linearly with g', and therefore is not fully predictable from the MO salinity (S_{MO}). It is conceivable that the effects of increased relative entrainment would tend to reduce the settling depth of glacial MO from the value expected purely on the basis of the change in g'. To overcome this uncertainty, it is important that the location of the LGM flow path of the MO is identified within the GoC.

2.2. Sedimentary Processes

[15] The Gulf of Cadiz contourite, formed as a result of the activity of the MO plume on the GoC slope, extends from Cape Spartel in the southeast to Cape St. Vincent in the northwest and the sediment generally fines toward the northwest and downslope, as the current decelerates [*Kenyon and Belderson*, 1973]. Figure 2 shows an interpretation of side-scan sonar data for the GoC contourite drift, which can be divided into five parts [*Hernandez-Molina et al.*, 2003]. Four of these chart the declining velocity of the MO along the GoC margin.

[16] The southeastern area (region 1 in Figure 2), where the MO displays velocities of 1.4 m s^{-1} [*O'Neill-Baringer and Price*, 1999], is characterized by sand deposition, abrasion surfaces and erosional surfaces with rock outcrops [*Kenyon and Belderson*, 1973]. On the downslope flank of the drift in region 1, a high levee of sand marks the lower edge of the drift where the velocity of the MO decreases [*Hernandez-Molina et al.*, 2003]. Current meter studies show that some water spills over the levee, passing further downslope to contribute to the lower (MO2) flow [*O'Neill-Baringer and Price*, 1999]. Offshore Cadiz, between regions 1 and 3, the flow becomes complicated by the accentuated topography. The Cadiz and Guadalquivir Ridges deflect the MO for a short distance downslope in the area north of the Gil Eanes channel (Figure 2).

[17] Regions 3 and 4 (Figure 2) are characterized by branching and anastomosing channels, and include the areas of maximum contourite deposition (e.g., the Faro drift). Though the MO is forced to spread and split by the ridges it passes over in this region, most of the flow coalesces before it rounds Cape St. Vincent, forming MO1 [*Iorga and Lozier*, 1999]. In the most distal region 5 (Figure 2) much of the MO has lifted off the sediment surface, and the velocity has dropped sufficiently for mud-dominated deposition to occur (0.3–0.6 m s^{-1} [*O'Neill-Baringer and Price*, 1999]). This area is characterized by muddy sediment drifts dissected by large canyons.

[18] The overspill lobe sector (region 2 in Figure 2), hereafter referred to as the Gil Eanes Drift and which includes the Gil Eanes channel, is different in character. The Gil Eanes channel is a 1.5–3 km wide downslope channel that extends 40 km downslope between 900 and 1500 m water depth. MO water that has spilt over the levee of the main sediment drift (region 1) slowly descends the slope in this area (<0.5 m s^{-1} [*O'Neill-Baringer and Price*, 1999]) to form the deepest parts of MO2 [*Iorga and Lozier*, 1999]. This coalesces with water cascading down the slope further north and finally settles at ~1500 m as it leaves the GoC [*Iorga and Lozier*, 1999]. Though some sand is transported down the axis of the Gil Eanes channel to form an irregular sand body at its termination today, most of the Gil Eanes Drift is characterized by muddy sediment deposition [*Habgood et al.*, 2003; *Hernandez-Molina et al.*, 2003].

3. Material and Methods

[19] Details of the cores used in this study are summarized in Table 1. Core D13898 was recovered from the distal part of the Gil Eanes Drift (Figure 2) and consists of mud

Table 1. Cores Used During This Study

Core Number	Corer	Latitude, N	Longitude, E	Depth, m	Bottom Environment
D13682	piston	35°52	7°10.5	1514	sandy lobe below sediment drift
D13686	piston	35°46.5	7°37	998	southern levee of Gil Eanes Channel
D13892	Kasten	35°47.01	7°43.02	1497	hemipelagic slope below sediment drift
D13896	giant piston	36°02.60	7°18.00	817	sand-mud drift
D13897	giant piston	35°58.04	7°18.05	969	muddy drift
D13898	giant piston	35°54.00	7°24.58	1111	muddy drift
D13899	giant piston	35°50.57	7°29.00	1179	muddy drift
D13900	giant piston	35°48.57	7°31.01	1297	termination of Gil Eanes Channel

that is visually homogeneous throughout. D13900 was recovered 13 km to the SW of D13898 (Figure 2) and consists of similar muddy material, except for an interval of very fine sand between ~2 and ~4 m depth. Core D13892 is a 2 m long kasten core taken from the GoC, to the west of the region of MO interaction with the seafloor. There is no evidence for the presence of turbidites, current-influenced deposition or hiatuses within this core. Cores D13686 and D13896 are sandy cores recovered from the southern levee of the Gil Eanes Channel and the uppermost part of the Gil Eanes Drift, respectively.

[20] For planktonic foraminiferal abundance counts, samples were disaggregated, washed and sieved to remove all material finer than 150 μm using demineralized water. Where necessary, samples were then split into suitable aliquots of at least 300 individuals for identification according to the taxonomy of *Hemleben et al.* [1989]. The data are presented as percentages of total planktonic foraminiferal number. The foraminiferal sample preparations were used to also obtain rough grain-size information, in the form of percentage weight of four grain-size fractions (<63 μm, 63–125 μm, 125–150 μm and >150 μm) for each sample. Petrological characteristics (abundance of mineral detritus, nature of mineral and other grains) were also observed in the >150, 125–150 and 63–125 μm fractions.

[21] All specimens selected for stable isotope analyses were washed and sonicated in methanol to remove surface contamination. Analyses were carried out on 7–15 individuals of *Neogloboquadrina pachyderma* (d) between sizes of 150 and 212 μm or 6–15 individuals of *Globigerina bulloides* from a 190 to 210 μm size window. Stable isotope analyses were carried out using a Europa Geo 2020 mass spectrometer with individual acid dosing. The stable carbon and oxygen isotope ratios are expressed as δ values, in per mil (‰), relative to the Vienna Peedee belemnite standard [*Coplen*, 1988, 1994].

[22] Radiocarbon datings have been performed on >6 mg of clean handpicked planktonic foraminifera from the >150 μm fraction (excluding the deep dwelling taxa *Globorotalia* and *Globigerina calida*). The analyses were undertaken via the NERC Radiocarbon Laboratory (NERC-RCL), at the University of Arizona NSF-AMS facility (Table 2). The datings have been calibrated using the OXCAL program (www.rlaha.ox.ac.uk/orau/oxcal.html). In the case of the dates older than 26 ka B.P., the *Bard et al.* [1998] polynomial calibration has been used.

[23] We have performed 10 AMS ^{14}C datings on core D13898. These were calibrated, using the midpoint of the OXCAL probability distributions as the age determination in each case, and dates of intervening samples were calculated by interpolation (Figure 3a). Five datings were produced for D13892, following the same procedures, and this information has been incorporated into the age-depth model shown in Figure 3c.

4. Origin of Deposits

[24] Core D13900 is located at the termination of the Gil Eanes channel and its composition is controlled by the rate of sediment transport down the axis of the channel. There is little evidence of turbidite activity in this location, nor on the entire Gil Eanes Drift [*Habgood et al.*, 2003]. Moreover, the deposit formed by the Gil Eanes channel thickens basinward, the channel does not branch and it has symmetrical sediment waves on its levees [*Habgood et al.*, 2003]. These observations are inconsistent with a gravity flow origin of these deposits, and the formation of the downslope channels in this area is consequently thought to be exclu-

Table 2. Stratigraphic Position of Radiocarbon Datings[a]

Sample Depth, cm	Conventional Radiocarbon Age	1σ	Predicted Calendar Age
	D13898		
0	5,227	42	5,500
100	8,615	55	9,270
220	11,642	89	13,480
300	12,796	73	15,190
380	14,716	86	17,200
480	16,480	120	19,390
608	17,600	110	20,600
834	19,340	120	22,600
1234	23,010	180	26,612[b]
1628	24,040	200	27,797[b]
	D13892		
8	5,647	45	6,010
56.7	10,429	56	11,210
71	10,868	59	12,040
110	10,868	58	12,660
173	14,353	76	16,800
	D13686		
17	4,336	66	4,450
42.2	24,455	193	32,183[b]
74	26,488	123	34,494[b]
83.6	26,074	125	34,037[b]

[a]Conversion from conventional to calendar years is done with the OxCal program. A 400 year reservoir correction has been used.
[b]Conversion is done using *Bard et al.* [1998] polynomial calibration.

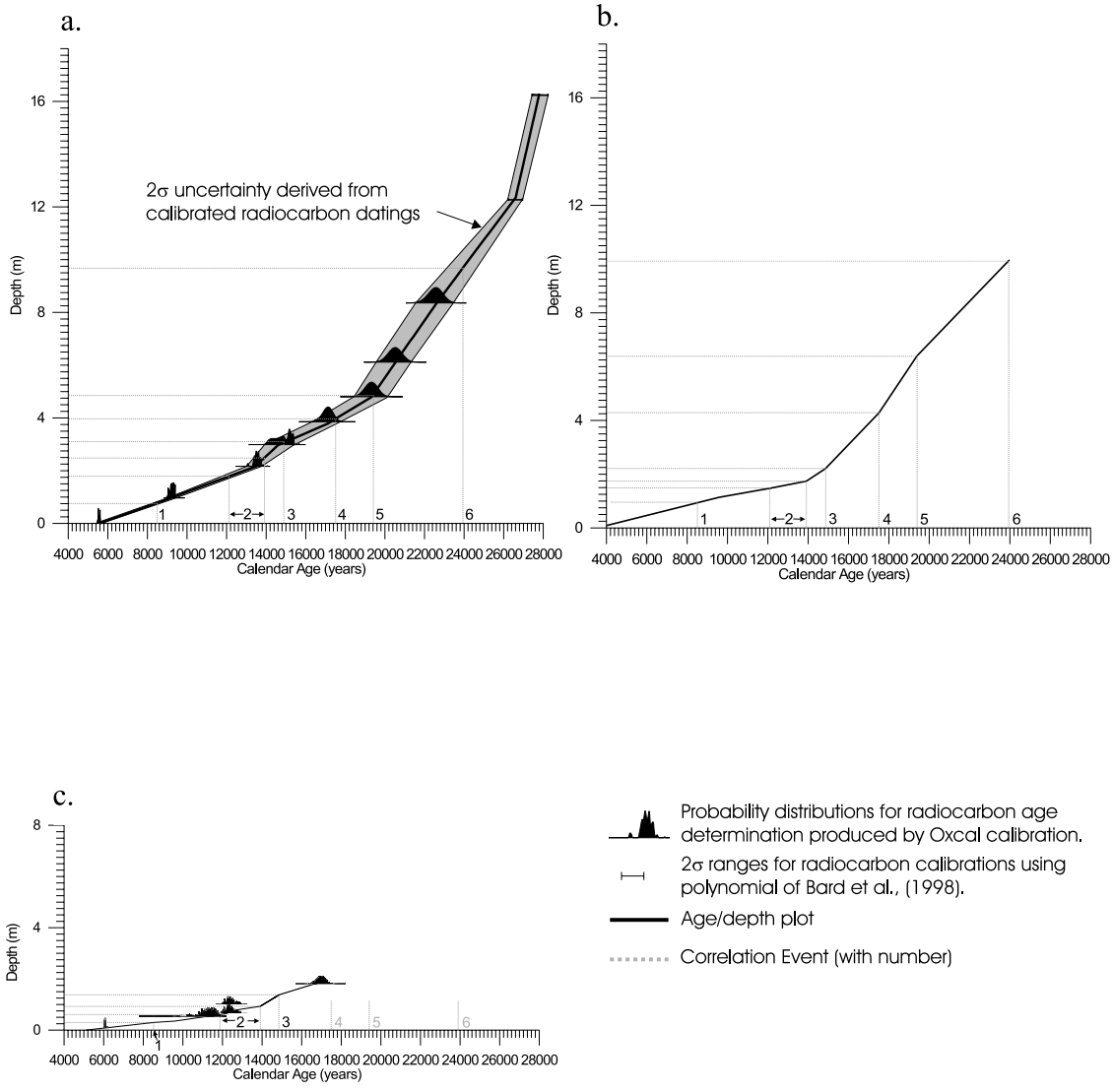

Figure 3. Accumulation rate in (a) D13898, (b) D13900, and (c) D13892 derived from relative correlation shown in Figure 4. Datings provided by radiocarbon age determinations are shown.

sively due to downslope flow of the MO [*Habgood et al.*, 2003]. D13898 lies on the northern side of the Gil Eanes channel, in a region of mud waves (Figure 2), where MO is active but not with sufficient velocity to transport sand. This core thus consists entirely of massive silty clay.

[25] In all samples from D13898 and D13900, the 63–125 μm fraction is petrologically similar, and it is also similar to other sandy samples taken from the Gil Eanes Drift (see Figure 2). It is siliceous with a high content of quartz and lithic fragments. There are many at least partly oxidized wood fragments and some samples also contain some soft, brown plant fragments. Benthic foraminifera are very abundant in the most sandy samples of D13900 (2.2–~4 m), and include many species characteristic of the shelf, such as *Planorbulina mediterranensis*, *Elphidium crispum* and *Ammonia beccarii* [*Murray*, 1991a, 1991b; *Villanueva-Guimerans and Cervera-Currado*, 1999]. This benthic foraminiferal assemblage and petrology is similar to that found in sandy sediments deposited at the termination of the Gil Eanes channel today (e.g., core top of D13682 [*Habgood et al.*, 2003], see "surface sand samples" in Figure 2), indicating that they originate from the same source. The down core stratigraphy of the cores studied is therefore considered to be predominately related to the activity (or absence) of the MO.

5. Chronostratigraphic Framework

[26] Planktonic foraminiferal $\delta^{18}O$ data and assemblage data for D13892, D13898 and D13900 are shown in Figure 4. Correlations have been made between these records on the basis of a series of six events recognized in the $\delta^{18}O_{N.\ pachyderma\ (d)}$ and planktonic foraminiferal assemblage records, which were dated by interpolation between

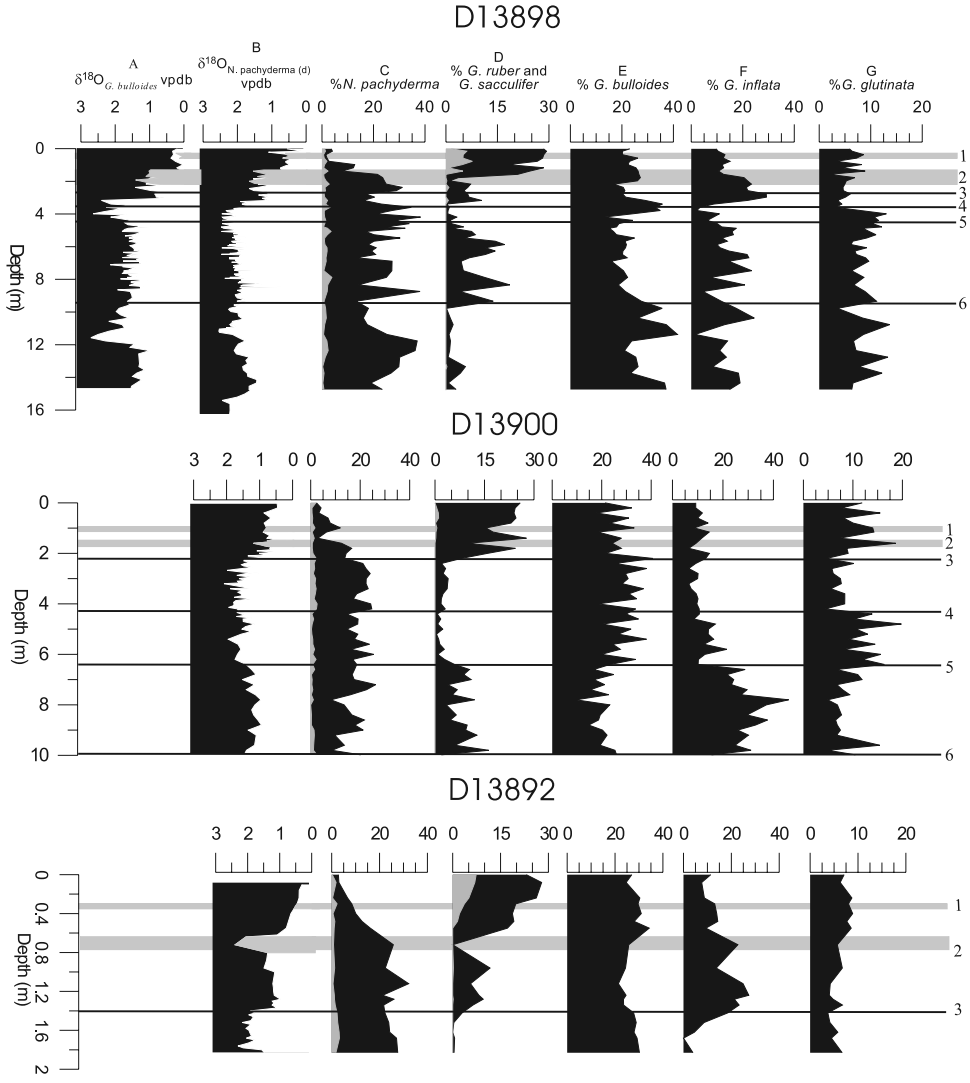

Figure 4. The $\delta^{18}O$ Vienna Peedee belemnite (VPDB) and planktonic foraminiferal abundance for D13898, D13900, and D13892: (a) $\delta^{18}O_{G.\ bulloides}$ VPDB, (b) $\delta^{18}O_{N.\ pachyderma\ (d)}$ VPDB, (c) *N. pachyderma* (dextral is black, sinistral is grey), (d) *G. ruber* (black) and *G. sacculifer* (grey), (e) *G. bulloides*, (f) *G. inflata*, and (g) *G. glutinata*. Events 1–6 represent strong events that can be recognized across these records: 1, local minimum in *G. ruber*, local maximum in *N. pachyderma* (d); 2, local maximum of *N. pachyderma* (d), local maximum in $\delta^{18}O$ VPDB, terminated with recovery of *G. ruber* and *G. sacculifer*; 3, decline in $\delta^{18}O$ VPDB, decline in *N. pachyderma* (d), increase in *G. ruber*; 4, increase in $\delta^{18}O$ VPDB, decline in *G. glutinata*; 5, collapse of *G. ruber* population, incoming of increase in $\delta^{18}O$ VPDB; and 6, decline in $\delta^{18}O$ VPDB, increase in *G. ruber*.

the 10 AMS ^{14}C datings in D13898 (Table 3 and Figure 3a). Although some diachroneity cannot be excluded, the majority of the selected events represent strong changes, and the distances between cores are rather small, so that near-synchronous behavior is expected. Figures 3b and 3c show age-depth relationships for D13900 and D13892 respectively, based on these correlations. All six events are recognized in D13900, which shows a similar accumulation rate history to D13898. Only events 1–3 are recognized in the shorter record of D13892, which extends back only to about 17 ka B.P. One radiocarbon dating in D13892 (110 cm, 12.66 ka) is inconsistent with the age model for this core as produced by correlation to D13898. The age of 12.66 ka B.P. estimated for this level seems excessively young, being identical to that of the dating at 71 cm, and interpolation from this date would lead to anomalous ages for events 2 and 3 relative to the datings in nearby core D13898 (Figure 4). To maximize comparability between D13892 and the other records in this study, the age determination provided by correlation is preferred, especially since event 3 is so clearly defined.

[27] Cores D13686 and D13896 (Figure 5) both largely consist of sand and sandy mud, and both have condensed upper parts displaying unconformities. In D13686, ~40 cm

Table 3. Correlation Points for D13898, D13900, and D13892

Event	Character	Age in D13898, years B.P.	Identification
1	local minimum in *G. ruber*, local maximum in *N. pachyderma* (d)	8,522	8.2 kyr event?
2	local maximum of *N. pachyderma* (d) and $\delta^{18}O$, terminates with recovery of *G. ruber* and *G. sacculifer*	12,135–13,909	Younger Dryas
3	decline in $\delta^{18}O$, decline in *N. pachyderma* (d), increase in *G. ruber*	14,861	termination 1a
4	increase in $\delta^{18}O$, decline in *G. glutinata*	17,508	
5	collapse of *G. ruber*, increase in $\delta^{18}O$	19,394	isotope stage 3/2 boundary?
6	decline in $\delta^{18}O$, recovery of *G. ruber*	23,937	

of sand overlie an unconformity which has been strongly discolored, probably by manganese growth. Such manganese mineral development is a recognized characteristic of condensed sedimentation under the influence of ocean bottom currents [*Stow and Lovell*, 1979; *Faugères and Stow*, 1993; *Shanmugam et al.*, 1993; *Stow et al.*, 1998]. Four radiocarbon datings are available for D13686 (Figure 5), produced in the same manner as in D13898. These datings indicate that the condensed postunconformity layer is of Holocene age (4.45 ka), while the underlying rhythmic sand/sandy mud is of glacial age (calibrated datings of 32183, 34037 and 34494 ka B.P. using the Bard et al. polynomial calibration method [*Bard et al.*, 1998]).

[28] Within D13898, D13892 and D13900, *G. sacculifer* is exclusively found in the Holocene, following its appearance around termination 1b (event 2, Figure 4). This has also been observed in other studies of cores from the GoC [*Sierro et al.*, 1999], and so appears to be a reliable regional chronostratigraphic event. Though the sands in D13686 and D13896 may have experienced significant reworking, this First Appearance event would still provide a maximum age estimate for this deposit. In D13686, the first appearance of *G. sacculifer* is noted at the unconformity, confirming that the condensed layer is of Holocene age (i.e., postunconformity deposition is at most 12 ka old).

[29] Further confirmation of a glacial age for the subunconformity deposits of D13686 is provided by the heavy $\delta^{18}O_{N.\ pachyderma\ (d)}$ values (1.5–2‰) throughout this core (Figure 5). The postunconformity deposit is characterized by values of $\delta^{18}O_{N.\ pachyderma\ (d)}$ around 0.8–1.5‰. Core

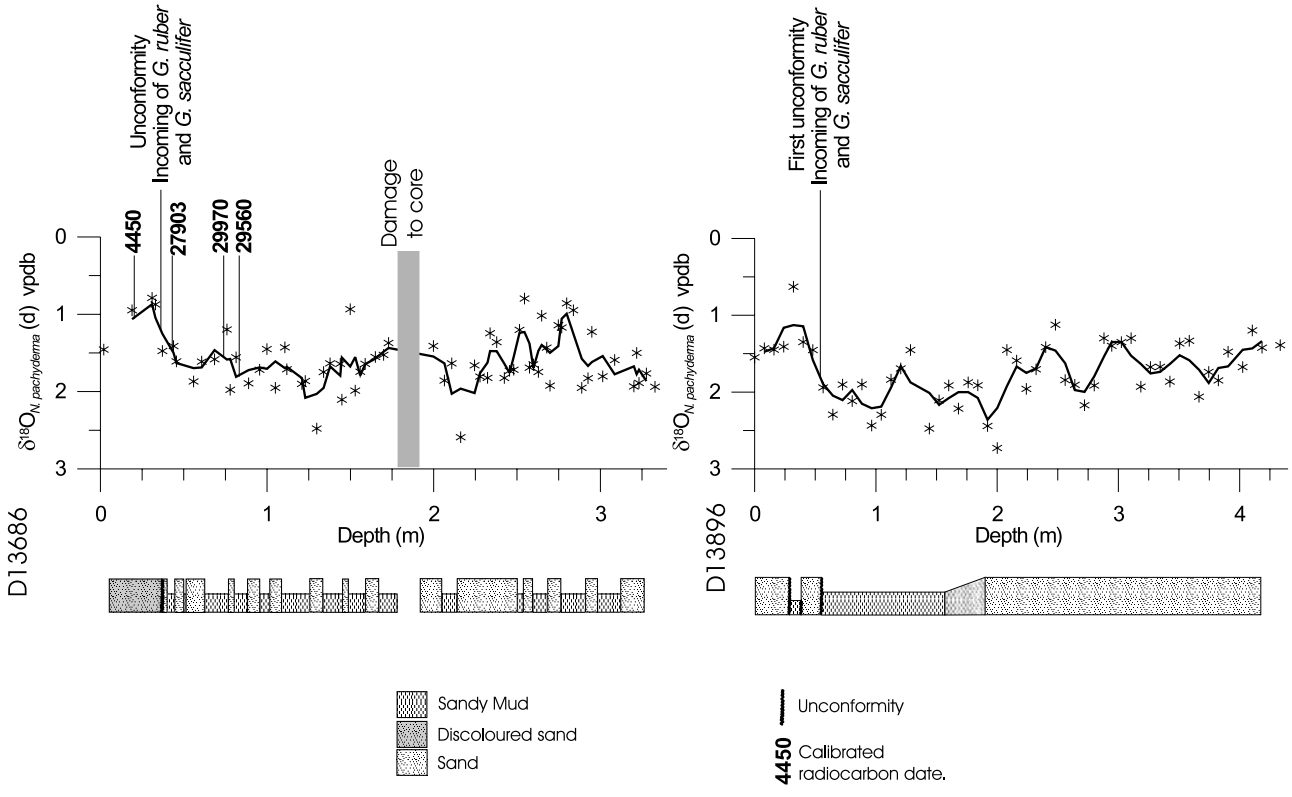

Figure 5. The $\delta^{18}O_{N.\ pachyderma\ (d)}$ VPDB, shown as three-point moving average and lithologies for sandy cores for D13896 and D13686.

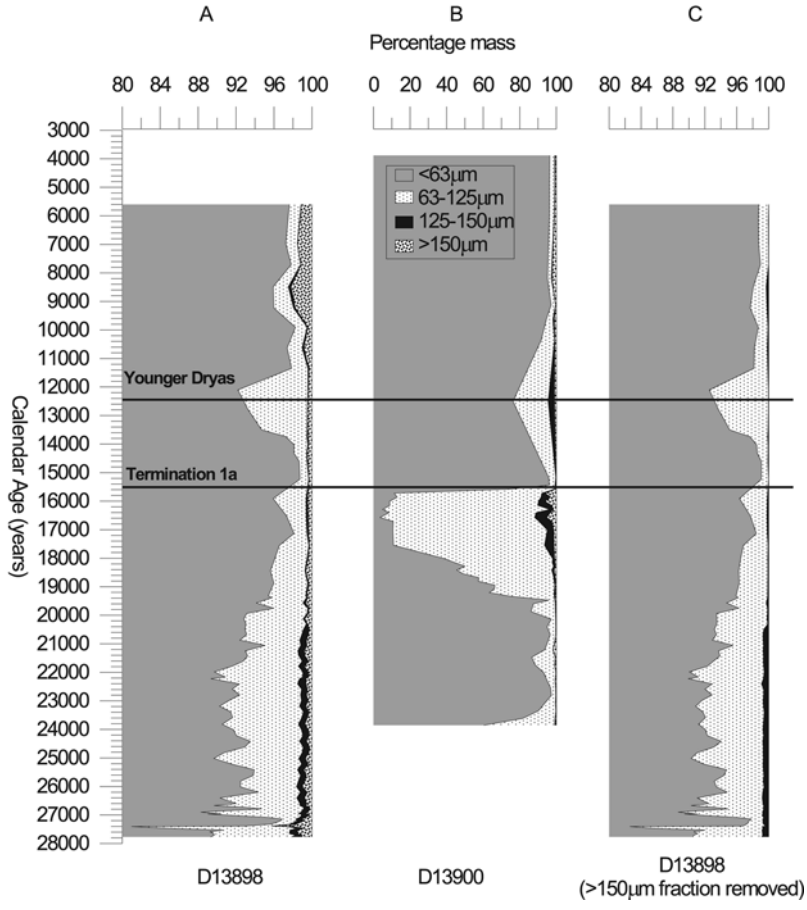

Figure 6. Grain size data for (a) D13898, (b) D13900, and (c) D13898. Each of the four grain-size fractions are represented as percentage of total dry mass. Figure 6c shows D13898 data as percentage of dry mass finer than 150 μm.

D13896 shows a similar signal to D13686 (Figure 5), in that $\delta^{18}O_{N.\ pachyderma\ (d)}$ decreases from glacial (1.5–2.5‰) to intermediate (~1‰) values at the unconformity, and the first appearance of *G. sacculifer* is recognized at this depth. It is concluded that D13896 and D13686 show similar deposition histories, so that the condensed upper part of D13896 represents the postglacial and the underlying sands and sandy muds represent glacial age deposition, as in D13686.

6. Results and Discussion

[30] The accumulation rate of core D13898 appears to gradually decrease up core (Figure 3a). The Holocene shows an accumulation rate that is only one fifth of that of the interval older than 25,000 years B.P. The upper parts of giant piston cores are often stretched during recovery [*Skinner and McCave*, 2003]. If that were the case in D13898, then an even stronger decrease of sediment accumulation would be inferred since the last deglaciation. Similar up-core reductions in accumulation rate are recognized in D13900 and D13892 (Figures 3b and 3c). Reduced accumulation on the Gil Eanes Drift during the Holocene relative to the last glacial period suggests that more sediment was being supplied to the Gil Eanes Drift prior to the last deglaciation and that less was being trapped further upslope than it is today. This would be consistent with previous suggestions that the MO current was less active at its modern position during the LGM than today [*Nelson et al.*, 1993].

[31] The 63–125 μm fraction of core D13898 almost exclusively consists of siliciclastic silt and very fine sand, whereas the >150 μm fraction is dominated by planktonic foraminiferal tests. The decreased rate of sediment accumulation in the Holocene of D13898 (Figure 4) caused a relative enrichment of planktonic foraminiferal number per gram of sediment, which explains the up-core increase in the relative importance of the >150 μm fraction weight (Figure 6a). To avoid this bias in D13898, we focus in this core on the grain-size changes within the fractions <150 μm (Figure 6c).

[32] Cores D13898 and D13900 both show increased sand deposition during the last glaciation relative to the Holocene (Figure 6), which is diagnostic of increased flow velocity at these locations at that time. Though they lack accurate datings, other giant piston cores (e.g., D13897 and

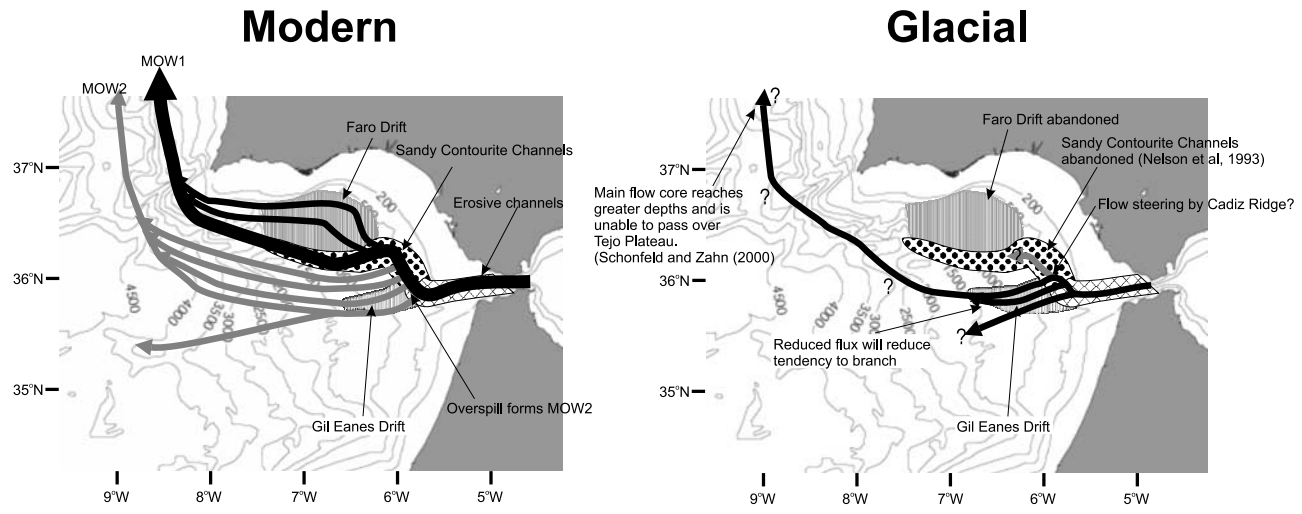

Figure 7. Position of the MO flow pathway today and interpretation of the pathway of the MO during the Last Glacial Maximum.

D13899, see Figure 2) from the same flank of the Gil Eanes Drift display similar down core grain-size trends to D13898, supporting the inference of enhanced glacial current velocities on the Gil Eanes Drift. Maximum sand content in D13900 occurs at ~17 ka B.P., roughly coincident with Heinrich event H1 and immediately subsequent to the LGM [*Rohling et al.*, 2003], while the lowest part of the core (>6 m depth, >20 ka B.P.), which is characterized by intermediate $\delta^{18}O_{N.\ pachyderma}$ values (~1.1‰), exhibits a sand content intermediate between that of the LGM and the Holocene. D13900 exhibits a very sharp fining at termination 1a, with the fraction >63 μm dropping from ~90% to ~10% of total mass (Figure 6). This rapid switch from sand to mud deposition reflects a dramatic decline in the amount of sand transported down the axis of the Gil Eanes channel, and suggests a sharp drop in current activity at the time of the deglaciation. D13898 shows a more gradual decline in sand content through this period, which may reflect that this core lies somewhat outside the direct transport pathway of the Gil Eanes Channel. Grain size at the D13900 location is affected by both current velocity and volume of sediment transport down the Gil Eanes Channel, and complicated by the impact of variation in transport on local sedimentary behavior. D13898 is unaffected by transportation down the Gil Eanes Channel, and it is therefore likely that D13898 more accurately reflects the velocity of the MO current.

[33] Core D13686 exhibits substantial sand deposition during the last glaciation, and this seems to be reflected also in D13896 (Figure 5). The supply of sand to both locations by the MO during the last glaciation supports the above interpretation of D13898 and D13900. Subsequent to the deposition of the sand layers in D13896 and D13686, at least one period of net erosion has occurred, and deposition during the Holocene is strongly condensed. These observations indicate that supply of sand to the Gil Eanes Drift has reduced considerably since the last glaciation, supporting inference of increased entrapment on the upper slope during the Holocene. The continued deposition of sand into the Holocene at D13686 and D13896 indicates that local energy remains too high for mud deposition to occur at these locations.

[34] Side-scan sonar data indicates the presence of small channels on the northern margin of the Gil Eanes Drift, positioned further from the high-energy core of water passing down the Gil Eanes Channel than D13896 and D13686 (north of D13896, Figure 2). However, cores recovered from these channels are capped with mud, and the sand recognized in the acoustic data is buried [*Habgood et al.*, 2003]. It is likely that these buried sands are of the same age as the sand recognized in D13896 and D13686, and therefore that the mud caps represent the Holocene. It can therefore be inferred that the width of the high-energy core passing down the Gil Eanes Drift has contracted since the last glaciation, and now is restricted to the immediate vicinity of the Gil Eanes Channel.

[35] The evidence presented above strongly suggests that the Gil Eanes Drift can be considered as a glacial age sandy drift that is now either becoming draped by Holocene mud, or receives only negligible net deposition. At glacial times, the Gil Eanes Drift appears to have been aggrading more rapidly, because of increased (sandy) sediment supply. Deposition occurred under the influence of an MO current that was locally more intense than it is today, and the width of the core of MO on the Gil Eanes Drift was increased relative to the Holocene. In contrast, activity of the MO on the upper slope was reduced, and other parts of the GoC sediment drift were abandoned. If the Gil Eanes Drift were accordingly interpreted as the main sediment drift deposited by the LGM Mediterranean Outflow, then that interpretation would be coherent with the expectation from physical arguments that the current should interact with a greatly reduced area of the seafloor, as a result of a smaller flux and reduced spreading. This interpretation is schematically illustrated in Figure 7.

[36] Our reconstruction agrees with the inference of strong flow on the Portuguese margin at 2000 m during the LGM [*Schönfeld and Zahn*, 2000]. Combined, this suggests that the settling depth of the main MO flow core,

which is ~800 m today [*Iorga and Lozier*, 1999], was nearer to ~2000 m at the LGM. In other words, the glacial MO settled to greater depths by roughly a factor of 2.5, compared to the present. This change is similar to the change in g', which we argue to have increased by a factor of about 2.4 on the basis of changes in the Gibraltar exchange [*Rohling and Bryden*, 1994].

7. Conclusions

[37] We infer an increase in the intensity of the MO current on the Gil Eanes Drift during the LGM, relative to the present. This corroborates our expectation based on physical constraints that the MO plume should at glacial times have settled at greater depths than today. Our reconstruction that the core of the flow passing over the Gil Eanes Drift had greater velocity and was wider during the last glaciation is consistent with a stronger focus of the MO down, rather than along, the GoC slope.

[38] The scale of the change in settling depth of the MO plume is comparable to the scale of the change in g' for MO water estimated from the constraint of the Gibraltar Exchange. We consequently view the past behavior of the MO to be primarily affected by the changing hydraulic control conditions in the Strait of Gibraltar, and consequently by sea level. At a depth of 2000 m, the shoaling of the MO plume in the northern North Atlantic would have been impeded; impacting on its ability to supply salt to the nascent North Atlantic Intermediate and Deep Waters and this may have negatively influenced the rate of Atlantic meridional overturning at glacial times. There is strong evidence that convection southwest of Iceland was an important part of the meridional circulation during glacial times [*Sarnthein et al.*, 1994, 1999]. The changing position and character of the MO would be anticipated to impact on this convection, potentially providing a controlling mechanism for where and when deep and intermediate water formation occurred during glacial times.

[39] **Acknowledgments.** We thank S. Cooke, M. Cooper, and M. Bolshaw for their invaluable assistance in stable isotope mass spectrometry and A. Hogg, H. Bryden, J. Thomson, and M. Siddall for stimulating discussions and feedback. We also thank J. Schönfeld for his comments on an early version of this manuscript and two anonymous reviewers whose comments further improved this paper. The radiocarbon datings were carried out as part of NERC-RCL project 949.1201.

References

Alves, M., F. Gaillard, M. Sparrow, M. Knoll, and S. Giraud (2002), Circulation patterns and transport of the Azores front-current system, *Deep Sea Res., Part II*, *49*, 3983–4002.

Armi, L., and N. A. Bray (1982), A standard analytical curve of potential temperature versus salinity for the western North Atlantic, *J. Phys. Oceanogr.*, *24*, 1295–1316.

Bard, E., M. Arnold, B. Hamelin, N. Tisnerat-Laborde, and G. Cabioch (1998), Radiocarbon calibration by means of mass spectrometric $^{230}Th/^{234}U$ and ^{14}C ages of corals: An updated database including samples from Barbados, Mururoa and Tahiti, *Radiocarbon*, *40*, 1085–1092.

Bigg, G. R. (1994), An ocean general circulation model of the glacial Mediterranean thermohaline circulation, *Paleoceanography*, *9*, 705–722.

Bigg, G. R. (1995), Aridity of the Mediterranean Sea at the Last Glacial Maximum: A reinterpretation of the $\delta^{18}O$ record, *Paleoceanography*, *10*, 283–290.

Borenas, K. M., A. K. Wahlin, I. Ambar, and N. Serra (2002), The Mediterranean Outflow splitting–A comparison between theoretical models and CANIGO data, *Deep Sea Res., Part II*, *49*, 4195–4205.

Bryden, H. L. (1993), Sill exchange to and from enclosed seas, in *Mediterranean Symposium*, edited by N. F. R. D. Croce, pp. 17–41, Inst. Sci. Ambientali Mar., Genoa, Italy.

Bryden, H. L., and T. Kinder (1991), Steady two-layer exchange through the Strait of Gibraltar, *Deep Sea Res., Part A*, *38*, S445–S463.

Bryden, H. L., and H. M. Stommel (1984), Limiting processes that determine basic features of the circulation in the Mediterranean Sea, *Oceanol. Acta*, *7*, 289–296.

Bryden, H. L., E. C. Brady, and R. D. Pillsbury (1988), Flow through the strait of Gibraltar, in *Seminario sobre la Oceanografia fisica del Estracho de Gibraltar*, edited by J. L. Almazan et al., pp. 166–194, Soc. Espan. de Estud. para la comun. fija a través del Estrecho de Gibraltar, Madrid.

Coplen, T. B. (1988), Normalization of oxygen and hydrogen isotope data, *Chem. Geol.*, *72*, 293–297.

Coplen, T. B. (1994), Reporting of stable hydrogen, carbon, and oxygen isotopic abundances, *Pure Appl. Chem.*, *66*, 273–276.

Faugères, J. C., and D. A. V. Stow (1993), Bottom-current-controlled sedimentation: A synthesis of the contourite problem, *Sediment. Geol.*, *82*, 287–297.

Gammelsrod, T. (1975), Instability of Couette flow in a rotating fluid and origin of Langmuir circulations, *J. Geophys. Res.*, *80*, 5069–5075.

Habgood, E., N. H. Kenyon, D. G. Masson, A. Akhmetzhanov, P. P. E. Weaver, J. Gardner, and T. Mulder (2003), Deep-water sediment wave fields, bottom current sand channels and gravity flow channel-lobe systems: Gulf of Cadiz, NE Atlantic, *Sedimentology*, *50*, 1–27.

Hall, I. R., and I. N. McCave (2000), Palaeocurrent reconstruction, sediment and thorium focussing on the Iberian margin over the last 140 ka, *Earth Planet. Sci. Lett.*, *178*, 151–164.

Hemleben, C., M. Spindler, and O. R. Anderson (1989), *Modern Planktonic Foraminifera*, 363 pp., Springer, New York.

Hernandez-Molina, J., et al. (2003), Looking for clues to palaeoceanographic imprints: A diagnosis of the Gulf of Cadiz contourite depositional systems, *Geology*, *31*, 19–22.

Hill, A. E., and E. G. Mitchelson-Jacob (1993), Observations of a poleward-flowing saline core on the continental slope west of Scotland, *Deep Sea Res., Part I*, *40*, 1521–1527.

Iorga, M. C., and M. S. Lozier (1999), Signatures of the Mediterranean Outflow from a North Atlantic climatology: 1. Salinity and density fields, *J. Geophys. Res.*, *104*, 25,985–26,009.

Johnson, G. C., R. G. Lueck, and T. B. Sanford (1994), Stress on the Mediterranean Outflow plume: part II. Turbulent dissipation and shear measurements, *J. Phys. Oceanogr.*, *24*, 2084–2092.

Johnson, J., I. Ambar, N. Serra, and I. Stevens (2002), Comparative studies of the spreading of the Mediterranean water through the Gulf of Cadiz, *Deep Sea Res., Part II*, *49*, 4179–4193.

Kenyon, N. H., and R. H. Belderson (1973), Bed forms of the Mediterranean undercurrent observed with side-scan sonar, *Sediment. Geol.*, *9*, 77–99.

Matthiesen, S., and K. Haines (2003), A hydraulic box model study of the Mediterranean response to postglacial sea-level rise, *Paleoceanography*, *18*(4), 1084, doi:10.1029/2003PA000880.

Moreno, E., N. Thouveny, D. Delanghe, I. N. McCave, and N. Shackleton (2002), Climatic and oceanographic changes in the northeast Atlantic reflected by magnetic properties of sediments deposited on the Portuguese margin during the last 340 ka, *Earth Planet. Sci. Lett.*, *202*, 465–480.

Mulder, T., et al. (2002), Studying past deep-ocean circulation and the paleoclimate record—Gulf of Cadiz, *Eos Trans. AGU*, *83*(43), 481, 487–488.

Murray, J. W. (1991a), Ecology and distribution of benthic foraminifera, in *Biology of Foraminifera*, edited by J. J. Lee and O. R. Anderson, pp. 221–253, Elsevier, New York.

Murray, J. W. (1991b), *Ecology and Paleoecology of Benthic Foraminifera*, Longman, New York.

Myers, P. G. (2002), Flux-forced simulations of the paleocirculation of the Mediterranean,

Paleoceanography, *17*(1), 1009, doi:10.1029/2000PA000613.

Myers, P. G., K. Haines, and E. J. Rohling (1998), Modeling the paleocirculation of the Mediterranean: The Last Glacial Maximum and the Holocene with emphasis on the formation of sapropel S_1, *Paleoceanography*, *13*, 586–606.

Nelson, C. H., J. Baraza, and A. Maldonado (1993), Mediterranean undercurrent sandy contourites, Gulf of Cadiz, Spain, *Sediment. Geol.*, *82*, 103–131.

Nelson, C. H., J. Baraza, A. Maldonado, J. Rodero, C. Escutia, and J. H. Barber (1999), Influence of the Atlantic Inflow and Mediterranean Outflow currents on late Quaternary sedimentary facies of the Gulf of Cadiz continental margin, *Mar. Geol.*, *155*, 99–129.

O'Neill-Baringer, M., and J. F. Price (1999), A review of the physical oceanography of the Mediterranean Outflow, *Mar. Geol.*, *155*, 63–82.

Pickard, G. L., and W. J. Emery (1990), *Descriptive Physical Oceanography: An Introduction*, 320 pp., Elsevier, New York.

Price, J. F., and M. O'Neill-Baringer (1994), Outflows and deep water production by marginal seas, *Prog. Oceanogr.*, *33*, 161–200.

Rahmstorf, S. (1998), Influence of Mediterranean Outflow on climate, *Eos Trans. AGU*, *79*(24), 281–282.

Reid, J. L. (1979), On the contribution of the Mediterranean Sea Outflow to the Norwegian-Greenland Sea, *Deep Sea Res., Part A*, *26*, 1199–1223.

Rodero, J., L. Pallares, and A. Maldonado (1999), Late Quaternary seismic facies of the Gulf of Cadiz Spanish margin: Depositional processes influenced by sea-level change and tectonic controls, *Mar. Geol.*, *155*, 131–156.

Rohling, E. J. (1994), Review and new aspects concerning the formation of Mediterranean sapropels, *Mar. Geol.*, *122*, 1–28.

Rohling, E. J. (1999), Environmental control on Mediterranean salinity and $\delta^{18}O$, *Paleoceanography*, *14*, 706–715.

Rohling, E. J., and H. L. Bryden (1994), Estimating past changes in the eastern Mediterranean freshwater budget, using reconstructions of sea level and hydrography, *Proc. K. Ned. Akad. Wet., Ser. B*, *97*, 201–217.

Rohling, E. J., and S. De Rijk (1999), Holocene climate optimum and Last Glacial Maximum in the Mediterranean: The marine oxygen isotope record, *Mar. Geol.*, *153*, 57–75.

Rohling, E. J., P. A. Mayewski, and P. Challenor (2003), On the timing and mechanism of millennial-scale climate variability during the last glacial cycle, *Clim. Dyn.*, *20*, 257–267.

Sarnthein, M., K. Winn, P. Jung, J. C. Duplessy, L. Labeyrie, H. Erlenkeuser, and G. Ganssen (1994), Changes in east Atlantic deepwater circulation over the last 30,000 years: Eight time slice reconstructions, *Paleoceanography*, *9*, 206–267.

Sarnthein, M., et al. (1999), Fundamental modes and abrupt changes in North Atlantic circulation and climate over the last 60ky—Concepts, reconstruction and numerical modelling, in *The Northern North Atlantic: A Changing Environment*, edited by P. Scafer et al., pp. 45–66, Springer, New York.

Schönfeld, J., and R. Zahn (2000), Late glacial to Holocene history of the Mediterranean Outflow: Evidence from benthic foraminiferal assemblages and stable isotopes at the Portuguese margin, *Palaeogeogr. Palaeoclimatol. Palaeoecol.*, *159*, 85–111.

Shanmugam, G., T. D. Spalding, and D. H. Rofheart (1993), Process sedimentology and reservoir quality of deep-marine bottom-current reworked sands (sandy contourites): An example from the Gulf of Mexico, *AAPG Bull.*, *77*, 1241–1259.

Sierro, F. J., J. A. Flores, and J. Baraza (1999), Late glacial to recent palaeoenvironmental changes in the Gulf of Cadiz and formation of sandy contourite layers, *Mar. Geol.*, *155*, 157–172.

Skinner, L. C., and I. N. McCave (2003), Analysis and modelling of gravity- and piston coring based on soil mechanics, *Mar. Geol.*, *199*, 181–204.

Stow, D. A. V., and J. P. B. Lovell (1979), Contourites: Their recognition in modern and ancient sediments, *Earth Sci. Rev.*, *14*, 251–291.

Stow, D. A. V., J. C. Faugères, and E. Gonthier (1986), Facies distribution and textural variation in Faro Drift contourites: Velocity fluctuation and drift growth, *Mar. Geol.*, *72*, 71–100.

Stow, D. A. V., J. C. Faugeres, A. Viana, and E. Gonthier (1998), Fossil contourites: A critical review, *Sediment. Geol.*, *115*, 3–31.

Thomson, J., S. Nixon, C. P. Summerhayes, J. Schönfeld, R. Zahn, and P. Grootes (1999), Implications for sedimentation changes on the Iberian margin over the last two glacial/interglacial transitions from $(^{230}TH_{excess})_0$ systematics, *Earth Planet. Sci. Lett.*, *165*, 255–270.

Thunell, R. C., and D. F. Williams (1989), Glacial-Holocene salinity changes in the Mediterranean Sea: Hydrographic and depositional effects, *Nature*, *338*, 493–496.

Villanueva-Guimerans, P., and J. L. Cervera-Currado (1999), Distribution of Planorbulinacea (benthic foraminifera) assemblages in surface sediments on the northern margin of the Gulf of Cadiz, *Trabajos Inst. Esp. Oceanogr.*, *15*, 181–190.

J. W. Murray, E. J. Rohling, and P. P. E. Weaver, Southampton Oceanography Centre, European Way, Southampton, SO14 3ZH, UK.

M. Rogerson, Faculty of Geoscience, University of Utrecht, Budapestlaan 4, NL-3584 CD Utrecht, Netherlands. (rogerson@geo.uu.nl)